ACS APPLIED MATERIALS & INTERFACES

www.acsami.org

Research Article

All-in-One Piezo-Triboelectric Energy Harvester Module Based on Piezoceramic Nanofibers for Wearable Devices

Sang Hyun Ji, Wooyoung Lee,* and Ji Sun Yun*

Cite This: *ACS Appl. Mater. Interfaces* 2020, 12, 18609−18616

Read Online

ACCESS | Metrics & More | Article Recommendations

ABSTRACT: An all-in-one energy harvester module comprising a top piezoelectric layer, a bottom piezoelectric layer, and a middle triboelectric layer was fabricated based on flexible piezoceramic nanofibers to serve as a power source for wearable devices. The top and bottom piezoelectric layers were manufactured by modularizing electrospun piezoceramic nanofibers with an interdigitated electrode, and the energy harvesting characteristics were maximized by laminating the single modules in *z*-axis array arrangements. The triboelectric layer was manufactured by attaching polydimethylsiloxane on both sides of an electrode layer, and the energy harvesting characteristics were controlled according to the surface roughness of the triboelectric modules. The output voltages of the individual energy harvester modules of the all-in-one module were individually or integrally measured by hand pressing the lower and upper parts of the module. The all-in-one energy harvester module generated a maximum voltage (power) of 253 V (3.8 mW), and the time required to charge a 0.1 μF capacitor to 25 V was 40 s. The results of a simulated energy harvesting experiment conducted on the all-in-one energy harvester module showed that 42 LED bulbs arranged in the shape of the "KICET" logo could be turned on in real time without charging, and a mini fan consuming a power of 3.5 W was operated after charging a 10 μF capacitor for 250 s. This work shows the potential of the all-in-one module as an ecofriendly flexible energy harvester for operating wearable devices.

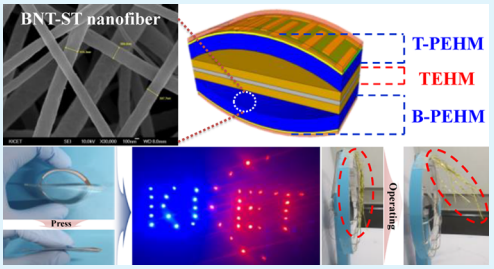

KEYWORDS: *energy harvesting, flexible all-in-one module, triboelectric, piezoelectric, nanofibers*

INTRODUCTION

Flexible piezoelectric ceramics have received attention as an environmentally friendly energy source for wearable devices because they can help convert unused mechanical energy into electrical energy regardless of the surrounding environment.[1−3] Although the brittleness and poor deformation characteristics of flexible piezoelectric ceramics have been overcome, the energy generated remains low.[4−6] To this end, hybrid energy harvester modules have been proposed, such as the piezoelectric−electromagnetic hybrid energy harvester module (HEHM),[7,8] piezoelectric−triboelectric HEHM,[9−11] and triboelectric−electromagnetic HEHM.[12] Among these HEHMs, piezo-triboelectric HEHMs are more suitable as a green energy source for wearable devices as they can not only generate high energy in response to human movements regardless of the surrounding environment but can also be manufactured easily and cost-effectively.

In piezo-triboelectric HEHMs, a hybrid module design has been studied to improve the module performance.[13−15] Improving the performance of each layer of the piezoelectric energy harvester module (PEHM) and triboelectric energy harvester module (TEHM) is also important. The PEHMs in recently developed HEHMs generally employ a top and bottom electrode with the d_{31} operating mode in which an electric field is formed vertically in the force direction.[14,15] To improve the piezoelectric characteristics, it is better to use an interdigitated electrode (IDE) with the d_{33} operating mode in which an electric field is formed horizontally in the force direction.[16,17] Furthermore, the output performance can be further improved by fabricating the multimodules in a single-module arrangement.[17] There have been many studies to improve the performance of TEHM.[18−22] Especially, with the increase in the surface roughness of the TEHM layer, more electrons are induced on the TEHM surface, thus improving the output characteristics.[23] In this regard, controlling the surface roughness can help improve the performance of TEHMs. Furthermore, PEHM and TEHM layers hybridized to an arch structure can help improve the output performance of HEHMs, including an increase in the curvature radius of the PEHM and increase in the contact area with the TEHM.[24]

Received: February 13, 2020
Accepted: April 6, 2020
Published: April 6, 2020

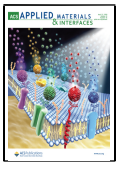

https://dx.doi.org/10.1021/acsami.0c02754
ACS Appl. Mater. Interfaces 2020, 12, 18609−18616

In this study, as a green energy source for wearable devices, an all-in-one HEHM comprising a top-PEHM (T-PEHM) layer, a bottom-PEHM (B-PEHM) layer, and a TEHM layer with an arch shape was prepared and characterized based on flexible piezoceramic nanofibers. The energy harvesting performance of the T-PEHM and B-PEHM layers fabricated using electro-spun piezoceramic nanofibers with an IDE was optimized by employing a *z*-axis array arrangement of the single modules. The surface roughness of the TEHM layer based on polydimethylsiloxane (PDMS) was controlled to improve the energy harvesting performance. The output voltages of the individual PEHM and TEHM of the all-in-one HEHM were measured individually or integrally. The all-in-one HEHM generated a maximum voltage (power) of 253 V (3.8 mW). Experimental results showed that 42 LED bulbs arranged in the shape of the "KICET" logo could be turned on in real time. The time required to fully charge a 0.1 μF capacitor to 25 V was found to be 40 s, and a mini fan with a power consumption of 3.5 W was operated after charging a 10 μF capacitor for 250 s.

RESULTS AND DISCUSSION

As shown in Figure 1a, the arch-shaped all-in-one HEHM structure comprises three layers: T-PEHM, B-PEHM, and TEHM. The T-PEHM and B-PEHM layers were prepared by the warm isostatic press (WIP) process of BNT-ST/PVDF ($0.78Bi_{0.5}Na_{0.5}TiO_3$−$0.22SrTiO_3$/poly(vinylidene fluoride-*co*-trifluoroethylene)) nanofibers and IDE, and the TEHM layer was prepared by attaching PDMS layers onto both sides of an electrode layer (aluminum foil). The all-in-one HEHM was fabricated by attaching the T-PEHM and B-PEHM layers onto the upper and lower parts of the TEHM layer with an arch shape, respectively. T-PEHM and B-TEHM were connected in series, and PEHM and TEHM were connected in parallel. Figure 1b shows the output voltages individually generated from the PEHM and TEHM layers and integrally generated from the all-in-one HEHM. The PEHM layers and TEHM layer generated output voltages of 6.7 and 205.4 V, respectively. As the PEHM was pressed, one large positive peak was first observed due to the mechanical displacement of the piezoelectric layer, and then, a small shoulder peak comes out while hitting the TEHM surface. However, when the pressing force was removed, it was detached at once, so only one negative peak without the shoulder peak was observed. The all-in-one HEHM with individual modules connected in parallel generated an output voltage of 214.5 V, and the output voltages generated from the individual module layers were integrated. Figure 1c shows the working process and charge transfer mechanism of the all-in-one HEHM according to the operating states. The synchronous measurement results of the individual module layers in the all-in-one HEHM were checked with the corresponding output signal simultaneously, and each part of the output signal was divided with respect to the related operating process as marked. In the initial state without any contact, no piezoelectric or triboelectric potential was generated. (i) In the contact state where the contact with the fingers begins, based on the coupling of the electrostatic induction and triboelectrification, the accumulated opposite charges on the BNT-ST/PVDF nanofiber surface of the PEHM and on the PDMS surface of the TEHM tended to be neutralized while approaching, which attracted compensated charges from the electrodes of the TEHM. The triboelectric energy was generated first in the TEHM owing to these electron movements. No piezoelectric energy was generated in the PEHM because of the insufficient displacement. (ii) In the full-contact state, the piezoceramic nanofibers were stressed because of the sufficient displacement and pressing force, and a maximum piezoelectric energy was generated. The PEHM with the IDE showed the d_{33} operating mode, yielding a much higher voltage than the piezoelectric module with the top and bottom electrode (d_{31} operating mode) at similar module dimensions. The induced electrostatic charges on the TEHM due to the electron movements were balanced, and the output value gradually decreased. (iii) In the separation state, a potential difference was generated again when the friction layer was separated, and the TEHM exhibited a maximum negative output voltage. (iv) In the full-separation state, although the output voltage of the TEHM decreased gradually as the potential difference was overcome, the PEHM generated a maximum negative output voltage because of the sufficient displacement. Furthermore, as the triboelectric charge is generally compensated faster than the piezoelectric charge while maintaining the residual deformation of the friction electric charge, the maximum output voltage in the TEHM was observed faster. After one cycle, the all-in-one HEHM returns to the initial state without generating energy until the external force and contact are applied again.

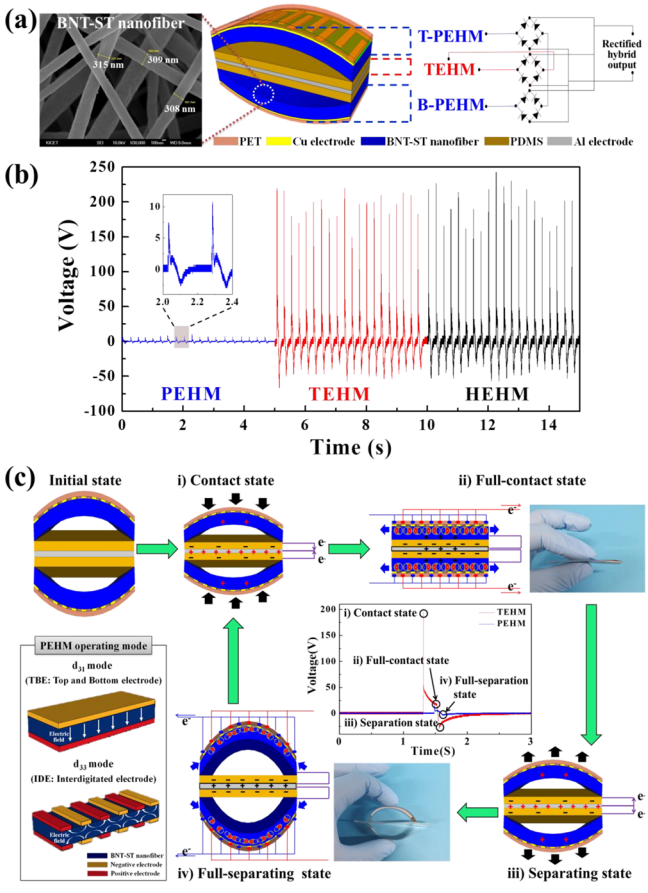

Figure 1. (a) Schematic of an all-in-one HEHM structure. (b) Output voltages of individual energy harvester modules of the HEHM. (c) Working principles of the HEHM according to operating states.

The material characteristics of the piezoceramic nanofibers in the T-PEHM and B-PEHM were investigated to evaluate the performance of the all-in-one HEHM, as shown in Figure

https://dx.doi.org/10.1021/acsami.0c02754
ACS Appl. Mater. Interfaces 2020, 12, 18609−18616

2. The XRD patterns of the piezoceramic nanofibers based on BNT-ST and PVDF-TrFE were measured in the 2θ range of

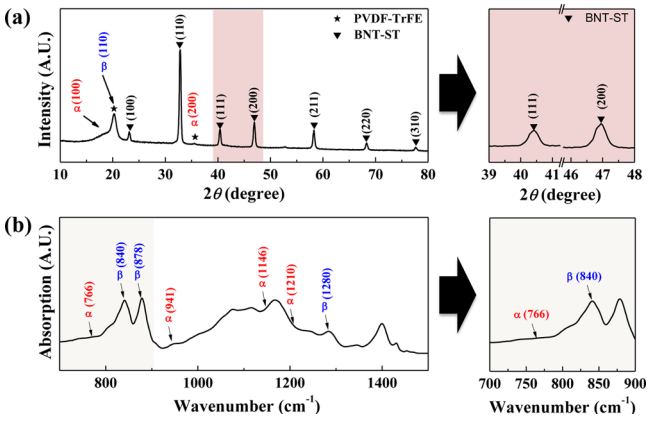

Figure 2. (a) XRD patterns and (b) FT-IR analysis spectra of the piezoceramic nanofibers based on BNT-ST and PVDF-TrFE.

20−80°, and three different crystal phase peaks can be observed, as shown in Figure 2a. BNT-ST piezoelectric ceramic peaks (JCPDS 89-3109) can be observed, and the (111) and (200) peaks between 40 and 47° can be observed as single peaks without separation, indicating the polarization of the BNT-ST ceramics distributed in the nanofibers by the electrospinning process.[25] The dominant β-phase (110) peak and the negligible α-phase (100, 200) peaks of PVDF-TrFE are observed. PVDF-TrFE copolymer polymers are semicrystalline polymers with five crystal phases such as α-, β-, γ-, δ-, and ε-phases. In general, α-phases dominate before the electrospinning process, while β-phases dominate after the electrospinning process because the dipoles are polled to one direction because of the high voltages applied during the electrospinning process.[26] In the FT-IR analysis, the absorption peaks at wavenumbers of 840, 878, and 1280 cm^{-1} indicate the β-phase of PVEF-TrFE, and the α-phase can be observed at wavenumbers of 766, 941, 1146, and 1210 cm^{-1}.[27] The β-phase content ($F(\beta)$) can be obtained using the equation based on Beer−Lambert's law.[28]

$$F(\beta) = A_\beta/\{(K_\beta/K_\alpha)A_\alpha + A_\beta\} \quad (1)$$

Here, A_α and A_β are the measured absorbances at 766 and 840 cm^{-1}, respectively, and K_α (6.1×10^4 cm^2/ mol) and K_β (7.7×10^4 cm^2/ mol) are the absorption coefficients at the respective wavenumbers. $F(\beta)$ was calculated to be 83%, indicating that the PVDF-TrFE of the piezoceramic nanofibers was well crystalized into the β-phase; therefore, good piezoelectric properties can be expected. The XRD and FT-IR results also show that PVDF-TrFE copolymers and BNT-ST piezoelectric ceramics coexist without affecting each other.

To improve the energy harvesting performance of the all-in-one HEHM, the performance of the PEHM layer was first optimized according to the number of PEHM layers with z-axis array structures connected in series, as shown in Figure 3a,b. In the case of a single PEHM, the output voltages (currents) of the individual T-PEHM, TEHM, and B-PEHM layers were 4.0 (1.5 μA), 204 (112 μA), and 3.4 V (1.0 μA), respectively, and the output voltage (current) of the integral HEHM layer was 211 V (115 μA). The overall energy in the all-in-one HEHM is believed to be integrally generated in the individual layers, and most of the energy is generated in the TEHM layer. Although there is a slight difference in the output voltages and currents of the T-PEHM and B-PEHM due to the difference in the forces acting from the top and bottom layers, the output behaviors are well matched. In Figure 3c, with the increase in the load resistance, the output currents of the T-PEHM, TEHM, and HEHM decrease; however, the maximum power is generated at a load resistance of 0.8 MΩ for the T-PEHM, 10 MΩ for the TEHM, and 0.9 MΩ for the HEHM. The overall load resistance of the HEHM was reduced due to the parallel connection of the rectified both PEHM and TEHM.[29] In general, the lower the resistance at which the maximum power is observed, the better its performance as a power source. Although the TEHM, which generates the most energy, shows the maximum power at a higher load resistance in the all-in-one HEHM, the maximum power is observed at a lower load resistance, similar to the resistance of the PEHM.

In other words, the advantage of the PEHM with the maximum power at a lower load resistance and the TEHM with the high output voltage can be integrally observed in the HEHM. With the increase in the number of modules making up the PEHM, the output voltages (currents) of the T-PEHM increase to 4.0 V (1.5 μA) for the single module, 5.2 V (2.9 μA) for the dual module, and 8.8 V (3.3 μA) for the triple module; the B-PEHM and T-PEHM show similar increasing trends, as shown in Figure 3a,b. However, a similar power density of 0.1 W/m^3 was observed, even though the number of PEHM layers increased. Although the amount of energy generated in the TEHM was not particularly affected, the output voltages (currents) of the all-in-one HEHM slightly increased to 211 V (115 μA) for the single module, 214 V (119 μA) for the dual module, and 219 V (121 μA) for the triple module. In general, the multiple modules based on the pure PEHM, which is not hybridized, showed increased output voltages and a similar output current with the increase in the number of series-connected modules.[16] In the case of the all-in-one HEHM, however, even when the individual PEHM layer was measured separately, the output voltage and output current of the PEHM increased with the number of modules connected in series. When separately measured, the contact between the PEHM and TEHM surfaces was unavoidable, and it is believed that the output current values increased because of the electron movements due to electrostatic induction. In the case of multiple PEHMs with over three layers, the low flexible characteristics not only make it difficult to manufacture the arch-shaped modules but also lead to poor structural stability because of repeated displacements. Therefore, the PEHMs in the all-in-one HEHM were optimized as a triple module structure.

To improve the energy harvesting performance of the all-in-one HEHM, the performance of the TEHM layer was optimized by controlling the surface roughness of the PDMS through a sanding and patterning process, as shown in Figure 4. In the all-in-one HEHM with the pure PDMS layer, a very flat PDMS surface can be observed from the AFM analysis, and the root mean square surface roughness (Rq) and the maximal average surface roughness (Rz) of the pure PDMS were approximately 30 and 40 nm, respectively. The PDMS surface of the all-in-one HEHM with the sanded PDMS layer showed a nanoscale surface roughness in the AFM image, and Rq and Rz values were found to be 30 and 240 nm, respectively, implying that the PDMS surface was rougher with a nanosize of approximately 210 nm. On the other hand, the PDMS surface of the all-in-one HEHM with the patterned PDMS

https://dx.doi.org/10.1021/acsami.0c02754
ACS Appl. Mater. Interfaces 2020, 12, 18609−18616

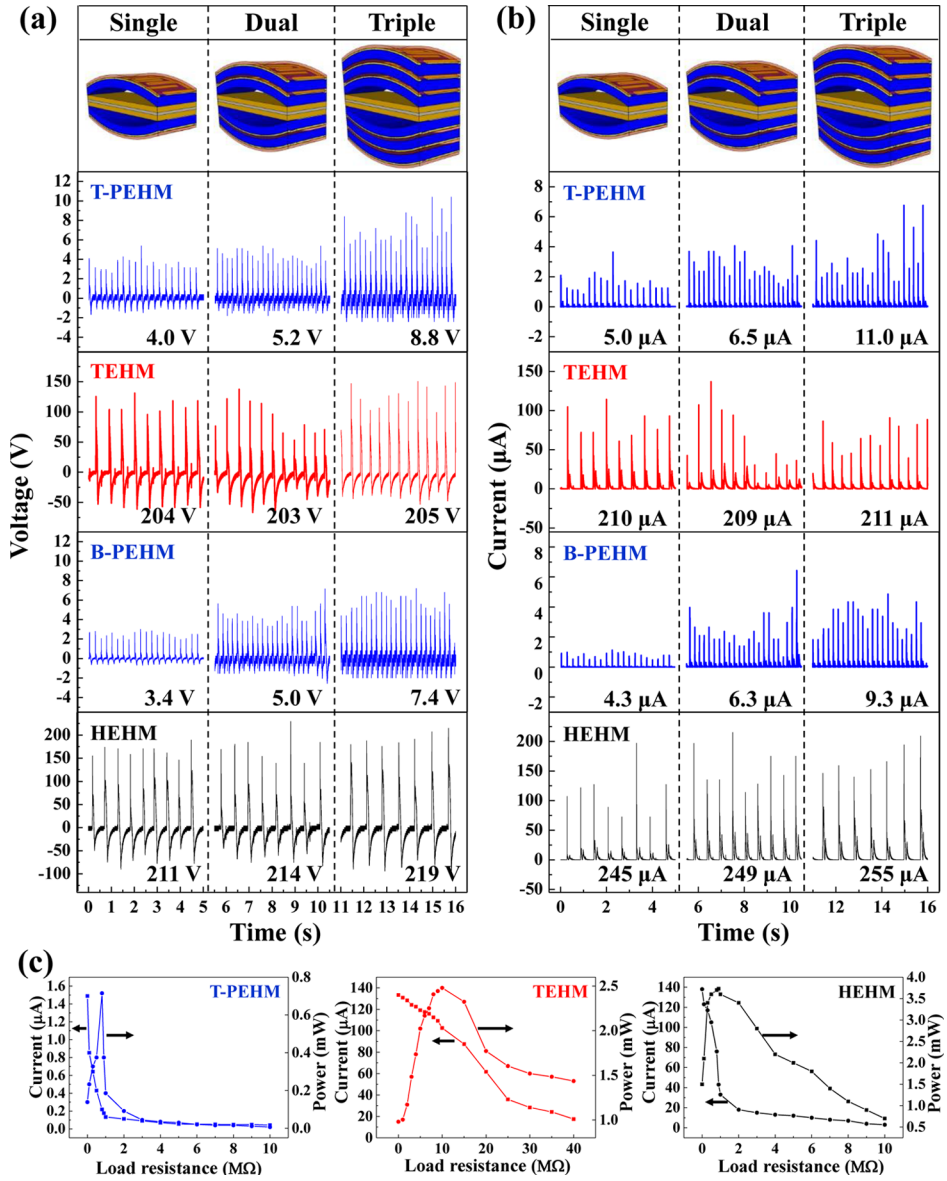

Figure 3. (a) Output voltages and (b) output currents of the all-in-one HEHM according to the module number of PEHM layers. (c) Output currents and power of the all-in-one HEHM with the single PEHM according to the load resistance.

layer showed a microscale surface roughness in the optical image with Rq and Rz values being approximately 1.30 and 6.40 μm, respectively. To have both nanoscale and microscale surface roughness, the PDMS surface of the all-in-one HEHM was sanded after patterning; the patterned and sanded PDMS have an Rq value of 1.28 μm and an Rz value of 6.43 μm. With the increase in the nanoscale surface roughness of the PDMS, the output voltage (currents) of the T-PEHM increased significantly from 9.9 V (3.3 μA) for the pure PDMS to 14.2 V (3.5 μA) for the sanded PDMS. The B-PEHM and T-PEHM showed similar tendencies. In the TEHM, the output currents (voltages) of the pure PDMS and sanded PDMS were 113 (202 V) and 138 μA (211 V), respectively. These results indicate that, as the surface roughness of the PDMS increases to nanoscale, although the output voltage of the TEHM increases slightly, the current output of the TEHM increases significantly. The high nanoscale surface roughness of the PDMS is believed to have contributed significantly to the increased output voltage of the piezoelectric layer because of the increase in the pressing pressure and the increase in the output current of the triboelectric layer due to increased contact surface area. The enhanced characteristics of each layer were coupled in the all-in-one HEHM, thus significantly improving the output voltage from 219 to 236 V and the output current from 128 to 143 μA with the increase in the nanoscale surface roughness. With the increase in the microscale surface roughness of the PDMS, the output voltage (currents) is improved from 9.9 V (3.3 μA) for the pure PDMS to 21.6 V (3.8 μA) for the patterned PDMS because of the higher pressure resulting from the microscale surface roughness compared with the nanoscale surface roughness. The output voltage (current) of the TEHM was slightly improved from 202 V (113 μA) for the pure PDMS to 207 V (120 μA) for the patterned PDMS. As the surface area under microscale surface roughness is lower than that under nanoscale surface roughness, the increase in the output voltage and current of the TEHM was lower than that under nanoscale surface roughness. The overall output voltage of the all-in-one

https://dx.doi.org/10.1021/acsami.0c02754
ACS Appl. Mater. Interfaces 2020, 12, 18609−18616

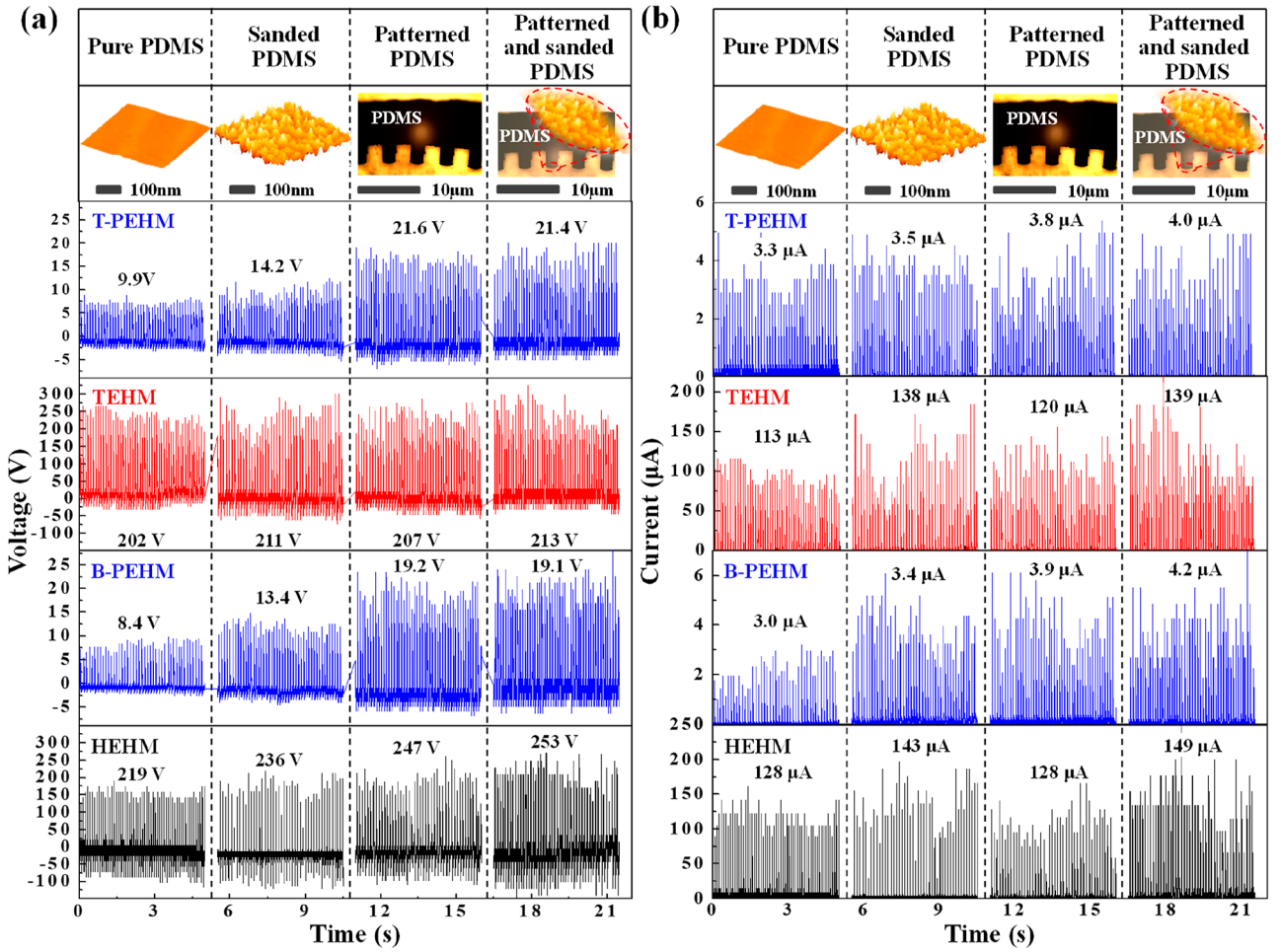

Figure 4. (a) Output voltages and (b) output currents of the all-in-one HEHM according to the surface roughness of the PDMS in the TEHM layer.

HEHM with a microscale surface roughness was higher than that with a nanoscale surface roughness because of the high improvement in the T-PEHM and B-PEHM layers by the increase of the pressing pressure. In contrast, the overall output current of the all-in-one HEHM with a nanoscale surface roughness was higher than that with a microscale surface roughness because of the high improvement in the TEHM layer by the increase of the contact surface area. In this regard, to improve the performance of both the piezoelectric and triboelectric layers, the all-in-one HEHM with nanoscale and microscale surface roughness was prepared by the patterning and sanding process. An output voltage of 253 V and an output current of 149 μA were obtained. In other words, the output characteristics of the TEHM layer were improved by controlling the TEHM surface with nanoscale roughness, and those of the PEHM layer were enhanced by adjusting the TEHM surface with the microscale roughness. As a result, the all-in-one HEHM generated maximum energy by controlling the nanoscale and microscale surface roughness.

When applying the HEHM to a wearable electronic device, the generated energy is generally used after charging a capacitor for a stable power supply to the device. A charge−discharge test was conducted, as shown in Figure 5a,b. The energy generated from the individual PEHM, individual TEHM, and all-in-one HEHM was used to charge 0.1, 1.0, and 10 μF capacitors for 100 s, as shown in Figure 5a. With the increase in the capacitance of the capacitor, the slope of the charge curve for each module decreases, and the PEHM with the lowest output voltage was unable to fully charge all the capacitors in 100 s. The TEHM and HEHM fully charged the 0.1 μF capacitors to 25 V, and the HEHM with the highest output voltage charged the 1.0 and 10 μF capacitors to 19.2 and 6.5 V in 100 s, respectively. Figure 5b shows the results of the charge−discharge tests conducted on the PEHM, TEHM, and HEHM for the 0.1 μF capacitor; the time required to charge the capacitor to 25 V is more than 200 for the PEHM, 50 s for the TEHM, and 40 s for the HEHM. Although there is no charge−discharge cycle for the PEHM due to the very low generated energy, the charge−discharge process of the TEHM and HEHM was linear with respect to time and showed good reversibility. Furthermore, the HEHM with a higher output voltage showed faster charging time than the TEHM. These results show that, by hybridizing the PEHM and the TEHM, the all-in-one HEHM not only exhibits an excellent charging durability but also a high charging speed, thus making it more applicable as a power source for wearable electronics. In the first simulated energy harvesting experiment conducted on the all-in-one HEHM, 42 LED bulbs arranged in the shape of the KICET logo turned on in real time without charging, as shown in Figure 5c. To make the KICET logo shape, 15 blue LED bulbs and 27 red LED bulbs were used, all of which were connected in a series. As the voltage required for illuminating

https://dx.doi.org/10.1021/acsami.0c02754
ACS Appl. Mater. Interfaces 2020, 12, 18609−18616

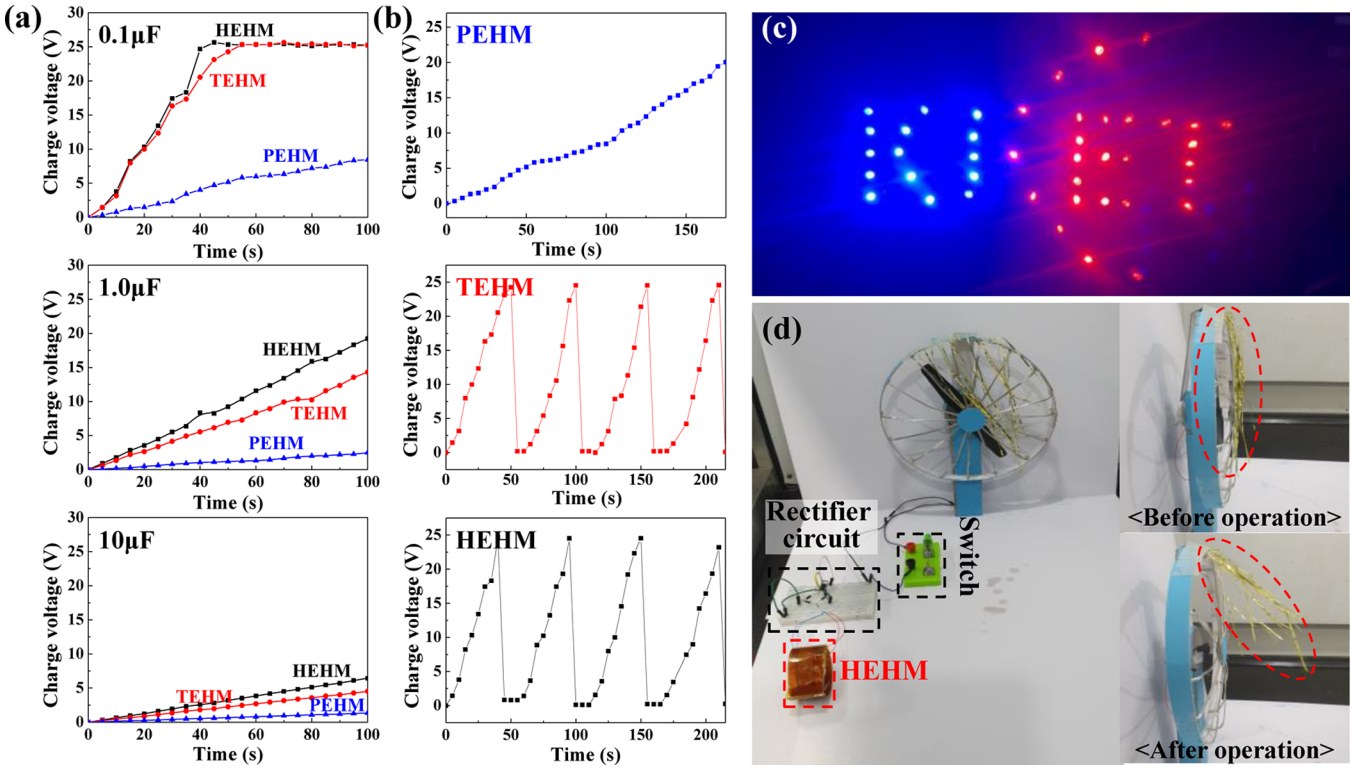

Figure 5. (a) Charge curves of 0.1, 1.0, and 10 μF capacitors. (b) Charge−discharge curves of the 0.1 μF capacitor for PEHM, TEHM, and HEHM. (c) 42 LED bulbs arranged in the KICET logo shape powered by the all-in-one HEHM in real time. (d) Operating images of a mini fan with a power consumption of 3.5 W after charging the 10 μF capacitor for 250 s using the all-in-one HEHM.

an LED bulb is about 2 V, an output voltage of 84 V or more was generated each time when pressing the all-in-one HEHM for illuminating the 42 LED bulbs in real time. Another simulated energy harvesting experiment was conducted in which a mini fan with a power consumption of 3.5 W was operated after charging a 10 μF capacitor for 250 s, as shown in Figure 5d. The HEHM was connected to a rectifier circuit with the capacitor. The mini fan operated well with the energy obtained from the capacitor when fully charged by pressing the HEHM continuously. With the two simulated energy harvesting experiments, we confirmed the feasibility of the all-in-one HEHM as an environmentally friendly flexible energy harvester for operating wearable devices.

CONCLUSIONS

An all-in-one HEHM structure with three layers, namely, a T-PEHM, a B-PEHM, and a middle TEHM layer with an arch shape, was manufactured based on flexible piezoceramic nanofibers as an ecofriendly flexible energy source for wearable devices. The flexible piezoceramic nanofibers in the PEHM were prepared by electrospinning and were modularized with IDEs using a WIP process. The energy harvesting performance of the PEHM was significantly improved by employing a *z*-axis array arrangement of the single modules, and the energy harvesting performance of the TEHM was controlled by regulating the surface roughness of the PDMS. Most of the energy was generated in the TEHM layer, and the load resistance, at which the maximum power is observed, was low in the PEHM layer. The all-in-one HEHM layer exhibited the advantages of the PEHM and TEHM layers. Charge−discharge tests conducted on the HEHM showed that it exhibits excellent charging durability and high charging speed. The all-in-one HEHM generated a maximum voltage (power) of 253 V (3.8 mW), and the time required to charge a 0.1 μF capacitor to 25 V was 40 s. The simulated energy harvesting experiments conducted on the all-in-one HEHM showed that 42 LED bulbs arranged in the shape of the KICET logo could be turned on in real time, and a mini fan with a power consumption of 3.5 W operated well after charging a 10 μF capacitor in 250 s. This work provides new insights into the design and application of flexible hybrid energy harvester modules as a green energy source for wearable devices.

EXPERIMENTAL PROCEDURE

To fabricate the PEHM layer, piezoceramic nanofibers were prepared by electrospinning and were modularized with the IDE using the WIP process.[16] High purity bismuth(III) oxide (Bi_2O_3), sodium carbonate (Na_2CO_3), titanium oxide (TiO_2), and strontium carbonate ($SrCO_3$) were purchased from Kojundo chemical, and poly(vinylidene fluoride-*co*-trifluoroethylene) (PVDF-TrFE) with a composition of 75/25 mol % was purchased from Measurement Specialties. Solvents of *N*,*N*′-dimethylformamide (DMF; 99.5%) and high purity acetone (99.995%) were purchased from Sigma-Aldrich. BNT-ST ($0.78Bi_{0.5}Na_{0.5}TiO_3-0.22SrTiO_3$) piezoceramics were prepared using a general solid-phase reaction method, and crystal structures of the BNT-ST nanofibers were analyzed by X-ray diffraction (XRD; max 2200 V, Rigaku Corporation) and Fourier transform infrared spectroscopy (FT-IR; ParkinElmer, Frontier 2/Spotlight 400). The BNT-ST powders (60 wt %) with a size of less than 20 μm were mixed in PVDF-TrFE solutions (PVDF-TrFE:DMF:acetone = 2:5:5). The homogeneous precursor solution was loaded into a 10 mL plastic syringe with a 21 G metal needle, and the needle was connected to a voltage power supply. A high voltage in the range of 10−15 kV was applied to the metal needle, and the precursor solution was supplied for 8 h at a rate of 1 mL/h. The BNT-ST nanofibers were electrospun onto a cylindrical drum collector located 10 cm from the needle tip

https://dx.doi.org/10.1021/acsami.0c02754
ACS Appl. Mater. Interfaces 2020, 12, 18609−18616

with a rotation speed of 1500 rpm at room temperature and 20−40% humidity. The IDE with an electrode width of 0.10 mm and an electrode interval of 0.20 mm was laminated onto one side surface of the BNT-ST nanofibers with a diameter of about 300 nm using the WIP process at 70 °C and 80 bar for 30 min, and the fabricated module with dimensions of 1 cm (W) × 5 cm (H) was poled at 1 kV for 1 h at room temperature.

To fabricate the TEHM layer, PDMS (Sylgard 184, Dow Corning Co.) and a curing agent were mixed at a ratio of 10 to 1 and then cured at 70 °C for 1 h. The cured PDMS layers were attached onto both sides of an electrode layer (aluminum foil) using a conductive epoxy. The surface roughness of the cured PDMS layer was controlled by the sanding or patterning process. The PDMS with nanoscale surface roughness was prepared by sanding the cured PDMS surface with 2000 grit sandpaper for 5 min. The PDMS with microscale surface roughness was fabricated by curing the PDMS solution on the substrate patterned to 1.2 μm at 80 °C for 1 h and then removing the patterned substrate. For fabrication of the PDMS with both nanoscale and microscale surface roughness, the PDMS solution was cured on the substrate micropatterned PDMS and then sanded the surface of the cured micropatterned PDMS to have nanoscale roughness. The surface microstructure of the PDMS layer was analyzed by atomic force microscopy (AFM; Nanostation II, SiS-GmbH) and optical microscopy (Olympus BX51 microscope), and the surface roughness was analyzed by surface profilometry (Surftest SJ-210; Mitutoyo Corporation, Aurora, IL) with a scan rate of 2 ps (1 μm/s) at a set point of 2.5 nN.

To fabricate the all-in-one HEHM, the T-PEHM and B-PEHM layers were attached onto the lower and upper parts of the TEHM layer with an arch shape, as shown in Figure 1a. T-PEHM and B-PEHM were connected in series, and PEHM and TEHM were connected in parallel. By hand pressing the lower and upper parts of the module, the output voltage and current of the module were recorded and measured using an oscilloscope (Tektronix, DPO 2012B) and a digital power meter (Yokogawa, WT 310), respectively. The output voltages of the individual energy harvester modules of the HEHM can be measured individually or integrally.

AUTHOR INFORMATION

Corresponding Authors

Wooyoung Lee − *Department of Materials Science & Engineering, Yonsei University, Seoul 03722, Republic of Korea;* orcid.org/0000-0001-8406-4324; Phone: 82-2-2123-2834; Email: wooyoung@yonsei.ac.kr; Fax: 82-2-312-5375

Ji Sun Yun − *Energy & Environmental Division, Korea Institute of Ceramic Engineering and Technology, Jinju 52851, Republic of Korea;* orcid.org/0000-0002-8528-6567; Phone: 82-55-792-2675; Email: susubin@kicet.re.kr; Fax: 82-55-792-2651

Author

Sang Hyun Ji − *Energy & Environmental Division, Korea Institute of Ceramic Engineering and Technology, Jinju 52851, Republic of Korea; Department of Materials Science & Engineering, Yonsei University, Seoul 03722, Republic of Korea*

Complete contact information is available at: https://pubs.acs.org/10.1021/acsami.0c02754

Notes

The authors declare no competing financial interest.

ACKNOWLEDGMENTS

This work was supported by the Industrial Technology Innovation Program (10079981; development of high efficiency lead-free energy harvesting materials and modules for wearable devices) funded by the Ministry of Trade, Industry and Energy (MOTIE) of Korea.

REFERENCES

(1) Chen, J.; Oh, S. K.; Nabulsi, N.; Johnson, H.; Wang, W.; Ryou, J.-H. Biocompatible and Sustainable Power Supply for Self-Powered Wearable and Implantable Electronics Using III-Nitride Thin-Film-Based Flexible Piezoelectric Generator. *Nano Energy* **2019**, *57*, 670−679.

(2) Maitra, A.; Karan, S. K.; Paria, S.; Das, A. K.; Bera, R.; Halder, L.; Si, S. K.; Bera, A.; Khatua, B. B. Fast Charging Self-Powered Wearable and Flexible Asymmetric Supercapacitor Power Cell with Fish Swim Bladder as an Efficient Natural Bio-Piezoelectric Separator. *Nano Energy* **2017**, *40*, 633−645.

(3) Chen, J.; Nabulsi, N.; Wang, W.; Kim, J. Y.; Kwon, M.-K.; Ryou, J.-H. Output Characteristics of Thin-Film Flexible Piezoelectric Generators: A Numerical and Experimental Investigation. *Appl. Energy* **2019**, *255*, 113856−113868.

(4) Shin, Y.-H.; Jung, I.; Noh, M.-S.; Kim, J. H.; Choi, J.-Y.; Kim, S.; Kang, C.-Y. Piezoelectric Polymer-Based Roadway Energy Harvesting via Displacement Amplification Module. *Appl. Energy* **2018**, *216*, 741−750.

(5) Lü, C.; Zhang, Y.; Zhang, H.; Zhang, Z.; Shen, M.; Chen, Y. Generalized Optimization Method for Energy Conversion and Storage Efficiency of Nanoscale Flexible Piezoelectric Energy Harvesters. *Energy Convers. Manage.* **2019**, *182*, 34−40.

(6) Jenkins, K.; Kelly, S.; Nguyen, V.; Wu, Y.; Yang, R. Piezoelectric Diphenylalanine Peptide for Greatly improved flexible Nanogenerators. *Nano Energy* **2018**, *51*, 317−323.

(7) Li, Z.; Li, T.; Yang, Z.; Naguib, H. E. Toward a 0.33 W Piezoelectric and Electromagnetic Hybrid Energy Harvester: Design, Experimental Studies and Self-Powered Applications. *Appl. Energy* **2019**, *255*, 113805−113817.

(8) Chou, X.; Zhu, J.; Qian, S.; Niu, X.; Qian, J.; Hou, X.; Mu, J.; Geng, W.; Cho, J.; He, J.; Xue, C. All-in-one filler-elastomer-based high-performance stretchable piezoelectric nanogenerator for kinetic energy harvesting and self-powered motion monitoring. *Nano Energy* **2018**, *53*, 550−558.

(9) Singh, H. H.; Khare, N. Flexible ZnO-PVDF/PTFE Based Piezo-tribo Hybrid Nanogenerator. *Nano Energy* **2018**, *51*, 216−222.

(10) Guo, Y.; Zhang, X.-S.; Wang, Y.; Gong, W.; Zhang, Q.; Wang, H.; Brugger, J. All-fiber Hybrid Piezoelectric-Enhanced Triboelectric Nanogenerator for Wearable Gesture Monitoring. *Nano Energy* **2018**, *48*, 152−160.

(11) Karumuthil, S. C.; Rajeev, S. P.; Varghese, S. Piezo-tribo Nanoenergy Harvester using Hybrid Polydimethyl Siloxane Based Nanocomposite. *Nano Energy* **2017**, *40*, 487−494.

(12) Hao, C.; He, J.; Zhai, C.; Jia, W.; Song, L.; Cho, J.; Chou, X.; Xue, C. Two-dimensional Triboelectric-electromagnetic Hybrid Nanogenerator for Wave Energy Harvesting. *Nano Energy* **2019**, *58*, 147−157.

(13) Sun, J.-G.; Yang, T.-N.; Wang, C.-Y.; Chen, L.-J. A Flexible Transparent One-Structure Tribo-piezo-pyroelectric Hybrid Energy Generator Based on Bio-Inspired Silver Nanowires Network for Biomechanical Energy Harvesting and Physiological Monitoring. *Nano Energy* **2018**, *48*, 383−390.

(14) Rodrigues, C.; Gomes, A.; Ghosh, A.; Pereira, A.; Ventura, J. Power-generating Footwear Based on a Triboelectric-Electromagnetic Piezoelectric Hybrid Nanogenerator. *Nano Energy* **2019**, *62*, 660−666.

(15) Shi, K.; Huang, X.; Sun, B.; Wu, Z.; He, J.; Jiang, P. Cellulose/$BaTiO_3$ Aerogel Paper Based Flexible Piezoelectric Nanogenerators and the Electric Coupling With Triboelectricity. *Nano Energy* **2019**, *57*, 450−458.

(16) Bowen, C. R.; Nelson, L. J.; Stevens, R.; Cain, M. G.; Stewart, M. Optimisation of Interdigitated Electrodes for Piezoelectric Actuators and Active Fibre Composites. *J. Electroceram.* **2006**, *16*, 263−269.

(17) Ji, S. H.; Yun, J. S. Optimization of a Flexible Piezoelectric Module Structure Based on a Lead-Free Piezoceramic Embedded in Nanofiber Composites. *Mech. Syst. Signal. Process.* **2020**, *136*, 106447.

(18) Zhang, X.-S.; Han, M.; Kim, B.; Bao, J.-F.; Brugger, J.; Zhang, H. All-in-one self-powered flexible microsystems based on triboelectric nanogenerators. *Nano Energy* **2018**, *47*, 410−426.
(19) Wen, D.-L.; Liu, X.; Deng, H.-T.; Sun, D.-H.; Qian, H.-Y.; Brugger, J.; Zhang, X.-S. Printed silk-fibroin-based triboelectric nanogenerators for multi-functional wearable sensing. *Nano Energy* **2019**, *66*, 104123−104133.
(20) Kim, I.; Jeon, H.; Kim, D.; You, J.; Kim, D. All-in-one cellulose based triboelectric nanogenerator for electronic paper using simple filtration process. *Nano Energy* **2018**, *53*, 975−981.
(21) Hou, X.; Zhu, J.; Qian, J.; Niu, X.; He, J.; Mu, J.; Geng, W.; Xue, C.; Chou, X. Stretchable Triboelectric Textile Composed of Wavy Conductive Cloth PET and Patterned Stretchable Electrode for Harvesting Multivariant Human Motion Energy. *ACS Appl. Mater. Interfaces* **2018**, *10*, 43661−43668.
(22) Qian, J.; He, J.; Qian, S.; Zhang, J.; Niu, X.; Fan, X.; Wang, C.; Hou, X.; Mu, J.; Geng, W.; Chou, X. A Nonmetallic Stretchable Nylon-Modified High Performance Triboelectric Nanogenerator for Energy Harvesting. *Adv. Funct. Mater.* **2019**, *30*, 1907414.
(23) Yu, J.; Hou, X.; Cui, M.; Zhang, S.; He, J.; Geng, W.; Mu, J.; Chou, X. Highly Skin-Conformal Wearable Tactile Sensor Based on Piezoelectric-enhanced Triboelectric Nanogenerator. *Nano Energy* **2019**, *64*, 103923−103937.
(24) Zhu, J.; Hou, X.; Niu, X.; Guo, X.; Zhang, J.; He, J.; Guo, T.; Chou, X.; Xue, C.; Zhang, W. The d-arched Piezoelectric-Triboelectric Hybrid Nanogenerator as a Self-Powered Vibration Sensor. *Sens. Actuators A Phys.* **2017**, *263*, 317−325.
(25) Ma, W.; Zhu, Y.; Marwat, M. A.; Fan, P.; Xie, B.; Salamon, D.; Ye, Z.-G.; Zhang, H. Enhanced Energy-Storage Performance with Excellent Stability Under Low Electric Fields in BNT−ST Relaxor Ferroelectric Ceramics. *J. Mater. Chem. C* **2019**, *7*, 281−288.
(26) Kim, S.-R.; Yoo, J.-H.; Park, J.-W. Using Electrospun AgNW/P(VDF-TrFE) Composite Nanofibers to Create Transparent and Wearable Single-Electrode Triboelectric Nanogenerators for Self-Powered Touch Panels. *ACS Appl. Mater. Interfaces* **2019**, *11*, 15088−15096.
(27) Hadimani, R. L.; Bayramol, D. V.; Sion, N.; Shah, T.; Qian, L.; Shi, S.; Siores, E. Continuous Production of piezoelectric PVDF Fibre for E-Textile Applications. *Smart Mater. Struct.* **2013**, *22*, 075017−075024.
(28) Mohammadi, B.; Yousefi, A. A.; Bellah, S. M. Effect of Tensile Strain Rate and Elongation on Crystalline Structure and Piezoelectric Properties of PVDF Thin Films. *Polym. Test.* **2007**, *26*, 42−50.
(29) Zhao, C.; Zhang, Q.; Zhang, W.; Du, X.; Zhang, Y.; Gong, S.; Ren, K.; Sun, Q.; Wang, Z. L. Hybrid piezo/triboelectric nanogenerator for highly efficient and stable rotation energy harvesting. *Nano Energy* **2019**, *57*, 440−449.

https://dx.doi.org/10.1021/acsami.0c02754
ACS Appl. Mater. Interfaces 2020, 12, 18609−18616